Autoionization versus photoionization of molecular adsorbates: CO_2 physisorbed on Ni(110)

T. Porwol, G. Illing, and H.-J. Freund
Lehrstuhl für Physikalische Chemie 1, Ruhr-Universität Bochum, Universitätsstrasse 150, 4630 Bochum, Federal Republic of Germany

H. Kuhlenbeck* and M. Neumann
Fachbereich Physik, Universität Osnabrück, Barbarastrasse 7, 4500 Osnabrück, Federal Republic of Germany

S. Bernstorff and W. Braun
Berliner Elektronenspeicherring-Gesellschaft, Lentzeallee 100, 1000 Berlin 33, Federal Republic of Germany

W. von Niessen
Institut für Physikalische und Theoretische Chemie, Technische Universität Braunschweig, Hans-Sommer Strasse 10, 3300 Braunschweig, Federal Republic of Germany

C.-M. Liegener
Institut für Physikalische und Theoretische Chemie, Universität Erlangen-Nürnberg, Egerlandstrasse 3, 8520 Erlangen, Federal Republic of Germany

(Received 24 May 1989)

We compare the cross sections for valence-electron photoionization and autoionization after C $1s$-to-bound and O $1s$-to-bound excitation of CO_2 physisorbed on Ni(110). Clear evidence is found for different selection rules for radiative excitation versus radiationless decay into the same ion states. All ion states that belong to the class of two-hole–one-particle states, in particular those in the inner-valence-electron regime, where the one-particle picture for photoionization is known to break down, are observed with very large intensities in autoionization spectra, but are hardly observable at all in photoionization. Combining photoionization and autoionization, we can characterize the ion-state wave functions according to their oxygen and carbon parentage. Differences between O $1s \rightarrow 2\pi_u$ and C $1s \rightarrow 2\pi_u$ decay into the normal single-hole states are discussed in terms of symmetry breaking via electron-hole localization and vibrational coupling in the core-to-bound excited state. Our interpretation is based on an *ab initio* Green's-function calculation for the ion states in the outer and inner valence regions followed by explicit calculations of the radiationless autoionization rates.

I. INTRODUCTION

Photoemission has failed so far to allow for detailed spectroscopic investigations of the region of inner valence ionizations of adsorbed molecules. From the viewpoint of the gas phase, the inner-valence region appears particularly interesting because here the simple one-electron picture of photoemission is known to break down.[1] In other words, instead of observing only two inner-valence ion states, for example the $3\sigma_g$ and $2\sigma_u$ states in CO_2—connected with the ionization of CO-σ-bond orbitals—a whole series of ion states, dominated by two-hole–one-particle configurations (shakeup states) is found experimentally.[2] Due to these difficulties, very few attempts have been made by photoelectron spectroscopy to investigate the inner-valence ionizations of adsorbed molecules.[3–5] Several groups have recently chosen a different approach to tackle this problem: Electron spectroscopy via autoionization of highly excited states of the adsorbate.[6–15] These highly excited states are populated via core-to-bound excitations with synchrotron radiation,[8,16] and radiationless decay into valence ion states of the adsorbate. This is shown schematically in Fig. 1 (second and third panels from the left). If the photoelectron spectrum is recorded with the same photon energy as the autoionization spectrum, the two spectra occur at the same kinetic energies (left panel, Fig. 1). Since the two spectroscopic methods probe the same set of ion states it appears natural to put the two sets of electron spectra on the same binding-energy scale. We have studied in the present paper photoionization and autoionization of CO_2 physisorbed on Ni(110). We have chosen this system for several reasons: CO_2 is a molecule whose adsorption behavior has been studied in some detail recently using angle-resolved photoelectron spectroscopy (ARUPS),[17] x-ray photoemission (XPS),[18] high-resolution electron-energy-loss spectroscopy (HREELS),[17,19] near-edge-absorption fine structure (NEXAFS),[18] and diffuse low-energy electron diffraction (DLEED) (Ref. 18) measurements. It is known that CO_2 can be physisorbed at liquid-nitrogen temperatures. The created adsorbate is two to three layers thick, as judged from the attenuation

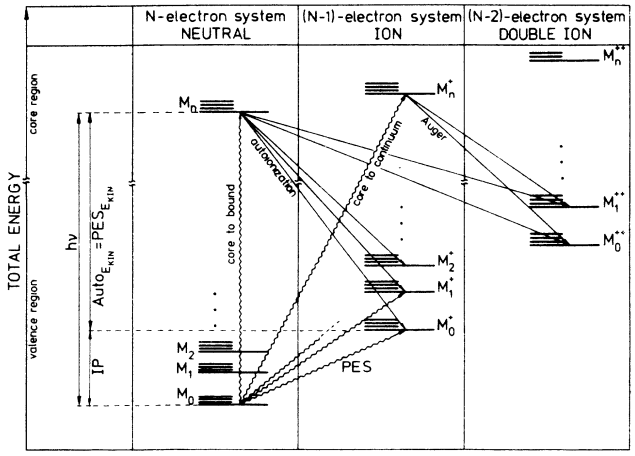

FIG. 1. Schematic total-energy-level diagram for ground and excited states of the neutral N-electron system (left panel), the single-hole-state $(N-1)$-electron system, and the double-hole state $(N-2)$-electron system. Wiggly arrows indicate photon excitations, straight arrows radiationless decay channels. The energy scale is broken in order to separate valence- and core-excited states.

of the substrate valence band.[17] The adsorbate is not a condensed layer in the classical sense because the coverage saturates. As reference for later studies, where we intend to study chemisorbed systems including coupling between adsorbate and metal surfaces, we neglect this coupling in the present case. This allows us to connect this study with previous works on the inner-valence ionization of CO_2 in the gas phase using photoelectron spectroscopy,[2] as well as with NEXAFS measurements, which probe the initial state of the autoionization decay. The present study is relevant to understand the lifetime of these core-to-bound excited states.[9] In addition, in photon-stimulated desorption from adsorbates, multielectron excitations, which can be assigned on the basis of the present technique, play a key role.[20]

II. EXPERIMENTAL DETAILS

The experiments were performed in two different magnetically shielded ultrahigh-vacuum systems containing facilities for low-energy electron diffraction (LEED), Auger spectroscopy (AES), residual-gas analysis with a quadrupole mass spectrometer, and photoelectron spectroscopy. The resolution was typically 1 eV. Excitation of photoelectrons was achieved by synchrotron radiation from the exit slit of a high-energy toroidal-grating monochromator (TGM) attached to the storage ring BESSY in Berlin. The base pressure in the system was below 10^{-8} Pa.

The Ni(110) crystal was spot welded to two tungsten rods mounted on a sample manipulator. With liquid nitrogen the crystal could be cooled to 85 K. Heating was possible by electron impact onto the reverse side of the crystal. The surface was cleaned by argon-ion bombardment. After annealing, the cleanliness was checked with AES, and surface order and geometry were established by LEED.

Upon adsorption of CO_2 (purchased from Linde AG, purity 99.999%) at all the temperatures used, no sharp LEED patterns were observed. Only the background of the sharp substrate LEED pattern appeared blurred upon adsorption. It turned out that interaction between CO_2 and the ion pump as well as the filaments of the ionization vacuum meter within a CO_2 pressure range 10^{-6}–10^{-4} Pa leads to formation of CO. Therefore, this pressure range was avoided. The ion pump and all filaments were switched off during admission of CO_2. The autoionization spectra shown in Fig. 2 are difference spectra. The spectrum of clean Ni has been subtracted from the adsorbate spectrum. In order to judge the difference spectra properly, it is important to realize that below 6 eV binding energy relative to E_f, the Ni spectrum can be represented by a flat line. Therefore, no artificial features are introduced in the spectra shown.

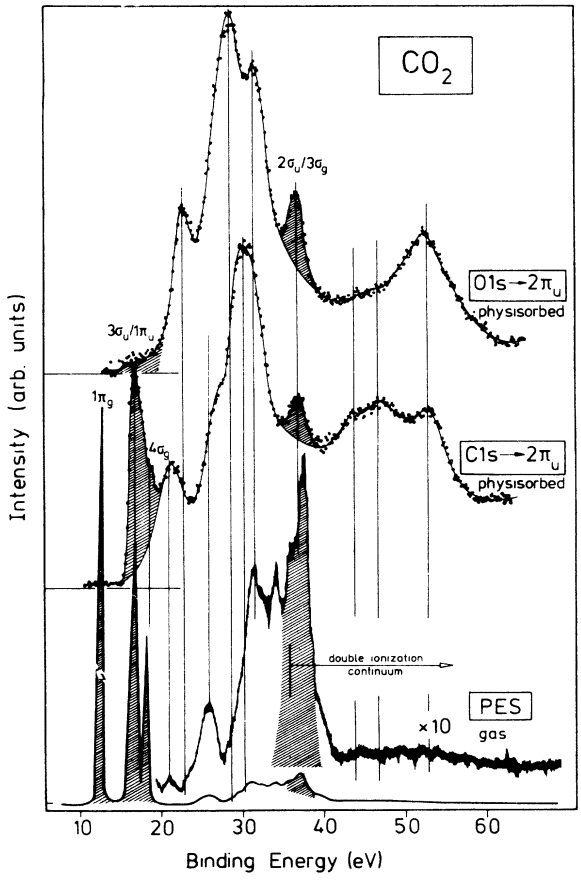

FIG. 2. Comparison of the autoionization spectra of physisorbed CO_2 on Ni(110) after C $1s \rightarrow 2\pi$ and O $1s \rightarrow 2\pi$ excitation with the gas-phase photoelectron spectrum of CO_2 (Ref. 2). The photoelectron spectrum has been shifted by 0.9 eV to lower binding energies (see text).

III. THEORETICAL DETAILS

The intensities measured in a photoelectron spectrum are governed by the following matrix elements if we adopt the sudden approximation:[21]

$$I \propto |\langle \Psi_f | \mathbf{A}\cdot\mathbf{p} | \Psi_i \rangle|^2 \approx \left| \sum_k \langle \Phi_f | \mathbf{A}\cdot\mathbf{p} | \Phi_k \rangle \langle \Psi_{\text{ion}}^n | a_k \Psi_i \rangle \right|^2 , \quad (1)$$

where Ψ_f and Ψ_i are initial and final states, respectively. Ψ_{ion}^n represents the nth final eigenstate of the ion. The Φ_k and Φ_f stand for the bound and continuum one-electron eigenstates, and a_k is the annihilation operator of the kth electron. $\mathbf{p}$ is the momentum operator and $\mathbf{A}$ the vector potential of the photon field. The energy differences, i.e., the ionization potentials, measured in a photoelectron spectrum, are determined by the difference of the total energies of the neutral system and of the ion. Both these quantities, the ionization energies and intensities, are calculated in the present paper via an *ab initio* Green's-function method. The Green's-function calculations are based upon *ab initio* self-consistent-field (SCF) calculations and include the effects of electronic correlation and reorganization. In view of the fact that we are particularly interested in the inner valence region, where satellite lines with appreciable intensities accompany the main lines, we have used the so-called extended two-particle-hole Tamm-Dancoff Green's-function method (extended 2ph-TDA). This method can be used in the entire valence region. It is accurate to third order in the electron-electron interaction and contains selected infinite summations such that the self-energy retains the correct analytical structure over the entire energy range.

TABLE I. Orbital energies (ε), extended 2ph-TDA ionization potentials (E_{IP}) (in eV), and pole strengths (P) for carbon dioxide. Only lines with $E_{\text{IP}} < 50$ eV and $P > 0.01$ are given.

	Ref. 29			This work			
Orbital	$-\varepsilon$	E_{IP}	P	$-\varepsilon$	E_{IP}	P	Assignment of the main configurations
$1\pi_g$	14.84	12.63	0.90	14.84	13.76	0.91	$1\pi_g^{-1}$
		38.45	0.01		36.74	0.01	$(1\pi_u^{-1}1\pi_g^{-1}2\pi_u)^{1,3}$ $(4\sigma_g^{-1}1\pi_g^{-1}6\sigma_g)^3$ $(4\sigma_g^{-1}1\pi_g^{-1}5\sigma_g)^1$ $(3\sigma_u^{-1}1\pi_u^{-1}6\sigma_g)^1$ $(3\sigma_u^{-1}1\pi_u^{-1}5\sigma_g)^3$ $(1\pi_u^{-1}1\pi_g^{-1}3\pi_u)^3$
$1\pi_u$	19.58	16.62	0.83	19.58	18.05	0.84	$1\pi_u^{-1}$ $(1\pi_g^{-2}2\pi_u)^1$
		22.75	0.01		22.48	0.02	$(1\pi_g^{-2}2\pi_u)^{1,3}$ $(1\pi_g^{-2}3\pi_u)^3$
		28.33	0.04		27.74	0.04	$(1\pi_g^{-2}2\pi_u)^{1,3}$ $(1\pi_g^{-2}3\pi_u)^3$ $1\pi_u^{-1}$ $(3\sigma_u^{-1}1\pi_g^{-1}6\sigma_g)^3$
		32.37	0.03		31.90	0.01	$(3\sigma_u^{-1}1\pi_g^{-1}5\sigma_g)^{1,3}$ $(4\sigma_g^{-1}1\pi_u^{-1}5\sigma_g)^3$ $(1\pi_g^{-2}3\pi_u)^3$ $(4\sigma_g^{-1}1\pi_u^{-1}6\sigma_g)^3$
$3\sigma_u$	20.27	16.83	0.89	20.28	18.56	0.90	$3\sigma_u^{-1}$
					36.97	0.01	$(4\sigma_g^{-1}3\sigma_u^{-1}5\sigma_g)^3$ $(4\sigma_g^{-1}3\sigma_u^{-1}6\sigma_g)^3$
$4\sigma_g$	21.79	18.12	0.87	21.79	19.86	0.88	$4\sigma_g^{-1}$
		33.68	0.01		26.93	0.01	$(3\sigma_u^{-1}1\pi_g^{-1}2\pi_u)^{1,3}$ $(4\sigma_g^{-1}1\pi_u^{-1}2\pi_u)^{1,3}$ $4\sigma_g^{-1}$
		36.39	0.02		32.95	0.01	$(3\sigma_u^{-2}6\sigma_g)$ $(3\sigma_u^{-1}1\pi_g^{-1}2\pi_u)^3$ $(1\pi_g^{-2}5\sigma_g)$ $(4\sigma_g^{-2}6\sigma_g)$
					36.54	0.01	$3\sigma_g^{-1}$ $(3\sigma_u^{-2}5\sigma_g)$ $(4\sigma_g^{-2}5\sigma_g)$ $(3\sigma_u^{-2}6\sigma_g)$ $(4\sigma_g^{-1}1\pi_u^{-1}2\pi_u)^3$ $(3\sigma_u^{-1}1\pi_g^{-1}2\pi_u)^1$
$2\sigma_u$	40.35	33.07	0.02	40.35	32.84	0.01	$(4\sigma_g^{-1}3\sigma_u^{-1}6\sigma_g)^3$ $(4\sigma_g^{-1}1\pi_g^{-1}2\pi_u)^3$ $(3\sigma_u^{-1}1\pi_u^{-1}2\pi_u)^3$ $(4\sigma_g^{-1}3\sigma_u^{-1}5\sigma_g)^3$
		34.40	0.03		34.22	0.06	$(1\pi_g^{-2}4\sigma_u)^1$ $2\sigma_u^{-1}$ $(1\pi_u^{-2}4\sigma_u)^1$
		35.30	0.54		34.51	0.01	$(1\pi_u^{-1}1\pi_g^{-1}5\sigma_g)^3$ $(1\pi_u^{-1}1\pi_g^{-1}6\sigma_g)^3$
		38.30	0.04		35.16	0.35	$2\sigma_u^{-1}$ $(1\pi_g^{-2}4\sigma_u)^1$ $(4\sigma_g^{-1}1\pi_g^{-1}2\pi_u)^1$
		38.76	0.03		36.26	0.01	$(1\pi_u^{-1}1\pi_g^{-1}6\sigma_g)^1$ $(1\pi_u^{-1}1\pi_g^{-1}5\sigma_g)^1$ $(4\sigma_g^{-1}1\pi_g^{-1}2\pi_u)^1$ $(4\sigma_g^{-1}3\sigma_u^{-1}5\sigma_g)^3$
		39.10	0.13		37.98	0.08	$(4\sigma_g^{-1}1\pi_g^{-1}3\pi_u)^{1,3}$ $(3\sigma_u^{-1}1\pi_u^{-1}3\pi_u)^{1,3}$ $2\sigma_u^{-1}$
		45.25	0.02		38.44	0.16	$2\sigma_u^{-1}$ $(4\sigma_g^{-1}1\pi_g^{-1}3\pi_u)^1$ $(3\sigma_u^{-1}1\pi_u^{-1}2\pi_u)^1$ $(4\sigma_g^{-1}1\pi_g^{-1}2\pi_u)^3$
					38.77	0.15	$(4\sigma_g^{-1}1\pi_g^{-1}3\pi_u)^3$ $2\sigma_u^{-1}$ $(3\sigma_u^{-1}1\pi_u^{-1}2\pi_u)^3$
$3\sigma_g$	41.78	33.18	0.01	41.78	32.95	0.01	$(3\sigma_u^{-2}6\sigma_g)$ $(3\sigma_u^{-1}1\pi_g^{-1}2\pi_u)^3$ $(1\pi_g^{-2}5\sigma_g)$ $(4\sigma_g^{-2}6\sigma_g)$
		35.39	0.22		35.15	0.15	$3\sigma_g^{-1}$ $(3\sigma_u^{-2}5\sigma_g)$ $(4\sigma_g^{-2}5\sigma_g)$ $(4\sigma_g^{-2}6\sigma_g)$ $(3\sigma_u^{-2}6\sigma_g)$ $(4\sigma_g^{-1}1\pi_u^{-1}2\pi_u)^1$ $(3\sigma_u^{-1}1\pi_g^{-1}2\pi_u)^3$
		36.84	0.26		36.54	0.18	$3\sigma_g^{-1}$ $(3\sigma_u^{-2}5\sigma_g)$ $(4\sigma_g^{-2}5\sigma_g)$ $(3\sigma_u^{-2}6\sigma_g)$ $(4\sigma_g^{-1}1\pi_u^{-1}2\pi_u)^3$ $(3\sigma_u^{-1}1\pi_g^{-1}2\pi_u)^1$
		37.96	0.01		37.67	0.01	$(3\sigma_u^{-1}1\pi_g^{-1}3\pi_u)^{1,3}$ $(4\sigma_g^{-1}1\pi_u^{-1}3\pi_u)^{1,3}$
		39.42	0.01		39.43	0.32	$3\sigma_g^{-1}$ $(1\pi_g^{-2}7\sigma_g)$
		39.83	0.20		40.31	0.16	$(1\pi_g^{-2}7\sigma_g)$ $3\sigma_g^{-1}$
		40.54	0.11				

For the expansion of the ionic-state wave functions, all single-hole (h), single-particle (p), 2h1p, and 2p1h configurations which arise in the given basis set are used. The mixing of configurations of different particle number in the Dyson equation introduces the ground-state correlation effects and leads to the implicit inclusion of double excitations. This method is extensively discussed in Ref. 22 (for an earlier version of this method, see Ref. 23). The multiroot Davidson method[24,25] is used to extract about 20–50 solutions for each symmetry, where the dimension of the matrices is about 2300. Some numerical aspects have been presented in Ref. 26. The Green's-function calculation is based on an SCF calculation which uses a large basis set including one set of d-type polarization functions,[27] namely $[11s5p1d]/(5s3p1d)$. [The exponential parameters of the d-type functions are $\alpha_d(\mathrm{C})=0.6$, $\alpha_d(\mathrm{O})=0.8$.] The SCF calculations were performed with the program MUNICH of Diercksen and Kraemer.[28] The orbital energies and the results of the extended 2ph-TDA calculation are shown in Table I. The orbital basis had to be slightly truncated in the extended 2ph-TDA calculation. The three core orbitals and their virtual counterparts, as well as virtual orbitals above 120 eV, have been neglected. For comparative purposes we show in Table I the result of an earlier, similar but slightly less extended, calculation by Domcke *et al.*[29]

For the calculation of the autoionization intensities we have to consider the following matrix elements according to Wentzel's ansatz:[30]

$$I_{ab} \propto \sum_{l,m} \sum_{\mu,\nu} c^*_{\mu b} c_{\nu b} \langle \mathbf{A}\Phi_\mu \Psi_{lm} | \mathbf{H} | \Phi_{ia} \rangle \langle \Phi_{ia} | \mathbf{H} | \mathbf{A}\Phi_\nu \Psi_{lm} \rangle \ , \tag{2}$$

where $\mathbf{H}$ is the Hamiltonian, and $\mathbf{A}$ the antisymmetrization operator. We have assumed in Eq. (2) that the states involved in the radiationless transition can be described by

$$|\Psi^a_{\mathrm{neutr}}\rangle = |\Phi_{1s\to 2\pi}\rangle \ , \tag{3}$$

$$|\Psi^b_{\mathrm{ion}}\rangle = \left| \mathcal{A} \sum_\mu c_{\mu b} \Phi_\mu \Psi_{lm} \right\rangle \ , \tag{4}$$

i.e., a single determinant representation for the core-to-bound excited neutral state, and a configuration interac-

TABLE II. Autoionization matrix elements for pure configurations (s, singlet coupled doublet state; t, triplet coupled doublet state).

	Wave function			
	C $1s\to 2\pi_u$		O $1s\to 2\pi_u$	
Configuration of the final state	CO_2	NO_2^+ (170°)	CO_2	COF^+ (170°)
$3\sigma_g^{-2}2\pi_u$	0.071 34	0.152 45	0.238 73	0.847 79
$s\ 3\sigma_g^{-1}2\sigma_u^{-1}2\pi_u$	0.078 33	0.145 67	0.319 67	0.078 78
$s\ 3\sigma_g^{-1}4\sigma_g^{-1}2\pi_u$	0.154 37	0.329 70	0.390 76	0.964 09
$t\ 3\sigma_g^{-1}4\sigma_g^{-1}2\pi_u$	0.000 00	0.007 82	0.129 83	0.365 93
$s\ 3\sigma_g^{-1}1\pi_u^{-1}2\pi_u$	0.119 20	0.216 75	0.203 04	0.742 50
$t\ 3\sigma_g^{-1}1\pi_u^{-1}2\pi_u$	0.062 58	0.113 41	0.092 42	0.340 16
$s\ 3\sigma_g^{-1}3\sigma_u^{-1}2\pi_u$	0.093 40	0.188 36	0.399 12	0.156 15
$s\ 3\sigma_g^{-1}1\pi_g^{-1}2\pi_u$	0.000 00	0.000 00	0.313 75	0.324 11
$s\ 2\sigma_u^{-1}4\sigma_g^{-1}2\pi_u$	0.119 85	0.222 22	0.368 35	0.060 51
$s\ 2\sigma_u^{-1}1\pi_u^{-1}2\pi_u$	0.178 90	0.281 73	0.190 13	0.045 81
$s\ 2\sigma_u^{-1}3\sigma_u^{-1}2\pi_u$	0.178 09	0.311 05	0.375 45	0.009 43
$s\ 2\sigma_u^{-1}1\pi_g^{-1}2\pi_u$	0.000 00	0.000 00	0.293 81	0.020 00
$4\sigma_g^{-2}2\pi_u$	0.167 02	0.356 50	0.342 16	0.673 02
$s\ 4\sigma_g^{-1}1\pi_u^{-1}2\pi_u$	0.182 39	0.330 65	0.276 30	0.781 59
$t\ 4\sigma_g^{-1}1\pi_u^{-1}2\pi_u$	0.095 75	0.173 58	0.093 49	0.207 71
$s\ 4\sigma_g^{-1}3\sigma_u^{-1}2\pi_u$	0.142 91	0.287 35	0.509 48	0.174 50
$s\ 4\sigma_g^{-1}1\pi_g^{-1}2\pi_u$	0.000 00	0.000 00	0.426 97	0.341 17
$1\pi_u^{-2}2\pi_u$	0.244 57	0.376 59	0.187 02	0.710 11
$s\ 1\pi_{ux}^{-1}1\pi_{uy}^{-1}2\pi_u$	0.272 24	0.419 41	0.209 54	0.795 82
$s\ 3\sigma_u^{-1}1\pi_u^{-1}2\pi_u$	0.213 32	0.364 30	0.300 21	0.147 87
$s\ 1\pi_u^{-1}1\pi_g^{-1}2\pi_u$	0.000 00	0.000 00	0.408 69	0.438 37
$3\sigma_u^{-2}2\pi_u$	0.150 15	0.284 41	0.383 63	0.024 02
$s\ 3\sigma_u^{-1}1\pi_g^{-1}2\pi_u$	0.000 00	0.000 00	0.463 91	0.064 55
$1\pi_g^{-2}2\pi_u$	0.000 00	0.000 00	0.446 57	0.135 31
$3\sigma_g^{-1}$	0.296 22	0.393 14	0.340 67	0.479 38
$2\sigma_u^{-1}$	0.232 86	0.261 38	0.322 81	0.032 08
$4\sigma_g^{-1}$	0.453 25	0.598 43	0.387 78	0.401 92
$1\pi_u^{-1}$	0.354 35	0.388 92	0.201 58	0.275 46
$3\sigma_u^{-1}$	0.277 65	0.337 99	0.393 14	0.059 86
$1\pi_g^{-1}$	0.000 00	0.000 00	0.311 49	0.120 24

tion representation for the final ion state. The coefficients in the configuration expansion are taken from the extended 2ph-TDA calculation. The Ψ_{lm} are spherical waves characterized by a set of angular momentum quantum numbers (l,m) describing the emitted electron, and centered at the core-hole site. Within this hierarchy of approximations, the calculation of the autoionization rates reduces to the calculation of a sum of two-electron integrals as shown in Ref. 31 of the type

$$\langle \chi_{1s}(1)\Psi_{lm}(2)|1/r_{12}|\chi_{v_1}(1)\chi_{v_2}(2)\rangle ,$$

where χ_{1s} and $\chi_{v1,2}$ represent one-electron orbitals of the $1s$ and the active valence electrons v_1 and v_2 involved, and Ψ_{lm} represents the outgoing electron. The integrals are evaluated according to the one-center approximation[32] employing the atomic radial integrals of McGuire.[33] We know from previous studies on diatomic molecules that a proper description of the screening process in the initial core-to-bound excited state is very important.[31] We have therefore used, as successfully done before,[31] equivalent core wave functions[34,35] to approximate the screened initial-state wave functions. In particular, to describe the initial state of the autoionization decay after C $1s$ excitation we use the SCF determinant of NO_2, after O $1s$ excitation the SCF determinant of COF. Note that while the equilibrium geometries of the latter systems are bent (NO_2: 134.25°) we have used almost linear (170°) geometries because CO_2 is a linear molecule. The bending by 10° facilitated the convergence of the SCF calculations. We take the result as representing the linear case. We have checked this for NO_2. For the SCF calculations of these species we employed minimal basis sets. This is reasonable, because only the one-electron wave functions, not their energies, enter the intensity calculations. Table II collects the calculated autoionization matrix elements for some selected configurations. In total, 72 configurations, all of which are either single-hole states or two-hole–one-particle configurations involving the $2\pi_u$ orbital, have been considered in the calculations. The 2h1p configurations involving other virtual orbitals have been neglected. However, some of the ion states, especially those at higher binding energies, contain these latter configurations. In all cases the vector of the configuration interaction coefficients has been renormalized, only considering configurations that contain the $2\pi_u$ orbital. This approximation is based on the assumption that the spectator electron is a pure $2\pi_u$ electron. The relatively narrow π resonance in the CO_2 NEXAFS spectrum[18] allows this conclusion to be drawn.

IV. RESULTS AND DISCUSSION

At the bottom of Fig. 2, the gas-phase photoelectron spectrum of CO_2 taken with $h\nu = 100$ eV in the range between 10 eV and 70 eV binding energy is shown.[2] The intensity scale of the spectrum above 20 eV binding energy has been multiplied by a factor of 10 in order to show the spectral features more clearly. This spectrum has to be compared with the computed photoelectron spectrum shown at the bottom of Fig. 3. It is quite clear that the bands below 20 eV binding energy, i.e., the $^2\Pi_g$, $^2\Pi_u$, $^2\Sigma_u$, and $^2\Sigma_g$ states of CO_2^+, representing electron emission from the $1\pi_g$, $1\pi_u$, $3\sigma_u$, and $4\sigma_g$ orbitals of CO_2, belong to the class of normal single-electron hole states. All other ion states observed are dominated by 2h1p configurations. Only the relatively intense features just below 40 eV binding energy supposedly contain a considerable amount of single-hole-state character due to coupling to the two CO_2-σ-bond orbitals which are situated in this energy range. As is obvious from the spectra, the intensity of the 2h1p states is rather low as compared to the single-hole states. It is even much lower for lower photon energies, and it does not increase far above the intensities observed in Fig. 2 for higher photon energies.[2] The reason for the relatively low intensity of the two-hole–one-particle states as compared to the single-particle states in photoemission is well known: 2h1p states, which are among the Ψ^n_{ion}-ion states in Eq. (4), gain intensity mainly by borrowing it from the single-hole states according to Eq. (1).[21] An assignment of the features in the photoelectron spectrum in Fig. 2, especial-

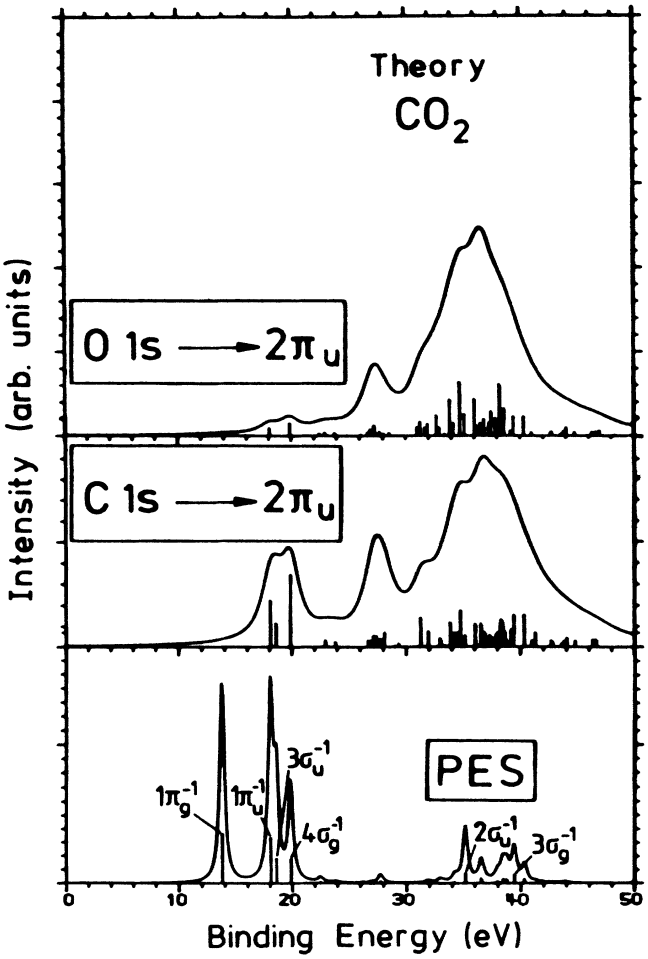

FIG. 3. Comparison of the calculated autoionization spectra after C $1s \rightarrow 2\pi_u$ and O $1s \rightarrow 2\pi_u$ excitation with the calculated photoelectron spectrum of CO_2.

ly in the 2h1p-state region, has been attempted on the basis of *ab initio* many-body calculations of Domcke *et al.*[29]: The three lowest-lying ion states in the 2h1p region are due to the three $^2\Pi_u$ states originating from the $1\pi_g^{-2}2\pi_u$ configuration, i.e., the HOMO-LUMO excitation, coupling to the $1\pi_u$-valence ion state. The low-energy states of the latter group have been assigned to the triplet-coupled doublet states, the high-energy states to the singlet-coupled doublet states. The present extended 2ph-TDA calculation corroborates the conclusions drawn earlier.

Both the previous and the present calculations suggest that the bands between 30 and 40 eV arise from $2\sigma_u$ and $3\sigma_g$ ionization. Six or seven rather intense components are distributed over 6–7 eV. Five of these have Σ_g and Σ_u character. The Σ_g states are calculated to have higher binding energies on the average compared with the Σ_u states. It is interesting to note that, according to both computations, the dominating configurations contributing to the wave functions of the Σ_u states do not involve excitations into the lowest unoccupied π orbital. Only rather high-lying unoccupied orbitals are involved in the configurations. In our previous photoemission study[2] we have assigned the two most intense peaks at 36.9 and 38 eV to the remnants of the $2\sigma_u$ and $3\sigma_g$, i.e., the CO σ-bond orbitals. These peaks are already situated beyond the double-ionization threshold situated at 36.4 eV in CO_2. Therefore, a strong mixing of these single-hole-state configurations with the double-ionization continuum must be expected. Below 40 eV we find a structured background but no intense features.

In the middle and at the top of Fig. 2 the autoionization spectra of CO_2 physisorbed on Ni(110) after C $1s\rightarrow 2\pi_u$ and O $1s\rightarrow 2\pi_u$ excitation are shown. The binding energies (see Table III) of the normal hole states found in the (C $1s\rightarrow 2\pi_u$)-autoionization spectrum are compatible with those determined via photoemission on a CO_2 physisorbate reported earlier (see Table III). They are rigidly shifted by 0.9 eV, as compared with the gas phase, which is due to a combination of polarization stabilization of the final ion state in the molecular solid,[37] and image potential screening by the metal. The initial state of the autoionization process has been studied via EELS in the gas phase by Wight and Brion,[38] and in the physisorbed phase by Illing *et al.*[18] using NEXAFS.

The discussion of the C $1s\rightarrow 2\pi_u$ autoionization spectrum shall proceed in two steps. The first step concerns autoionizations into the normal single-hole states below 20 eV binding energy. As is obvious from the comparison with the photoelectron spectrum, only the two bands due to ionization of the $1\pi_u/3\sigma_u$ and $4\sigma_g$ orbitals show up in the autoionization spectrum, while the $1\pi_g$ ionization, being the most intense one in photoemission, shows negligible intensity in autoionization. The reason is clear by considering the fact that two electron integrals determine the autoionization rate. A rule of thumb to evaluate the magnitude of the two-electron integrals is to consider the overlap between the strongly localized core hole

TABLE III. Binding energies (in eV) of CO_2 ion states. The asterisk indicates binding energies of CO_2 gas shifted by 0.9 eV.

	CO_2 gas		CO_2 physisorbed		
				Autoionization	
Ion state	PES[a]	Auger[b]	PES[c]	C $1s\rightarrow 2\pi_u$	O $1s\rightarrow 2\pi_u$
Π_g	13.8		12.9		
Π_u	17.3		16.4	16.6	broad
Σ_u	18.1		17.3		
Σ_g	19.4		18.5	18.7	
A	22.8		21.9*	21.5	
B	25.1		24.2*		22.7
C	26.9		26.0*	26.5	
D	29.8		28.9*		28.2
E	30.7		29.8*	30.4	
F	32.2		31.3*		31.1
G	33.4		32.5*		
H	35.0		34.1*	some intensity	
I	35.5		34.6*	but no peaks	
K	36.9		36.0*		36.7
L	38.0	38.0	37.1*	36.9	
M	40.6	39.4	39.7*		
O		43.5		43.5	
P		46.0		47.4	
		48.1			
Q		53.6		52.7	52.7

[a]See Ref. 2
[b]See Ref. 36.
[c]See Ref. 37.

and the delocalized valence electrons. The $1\pi_g$ one-electron state has, by symmetry requirements, vanishing atomic coefficients on the carbon center where the core hole is created. Consequently, the intensity of autoionization into the $^2\Pi_g$ states should, indeed, be small. The calculated autoionization spectrum shown in the middle of Fig. 3 reveals the above-discussed features, and basically explains this part of the experimental autoionization spectrum.

The second step concerns the two-hole–one-particle states above 20 eV binding energy. We have drawn correlation lines starting from the positions of the ion states in the inner valence region as determined from the high-resolution gas-phase study.[2] Obviously, compared with the region of single-hole states, the two-hole–one-particle states dominate the spectrum, i.e., they are the most intense bands in the spectrum. This general feature is well reproduced by the calculations shown in the middle of Fig. 3. A more detailed assignment has to be rather tentative even on the basis of the present involved calculations. We recognize the problem more clearly if measured and calculated spectra are plotted on the same energy scale as shown in Fig. 4: Between 20 and 25 eV binding energy, the calculation predicts two rather weak bands, with almost equal intensities due to autoionization into the $^2\Pi_u$ states, which show up in the photoelectron spectrum as weak satellites and have been assigned above

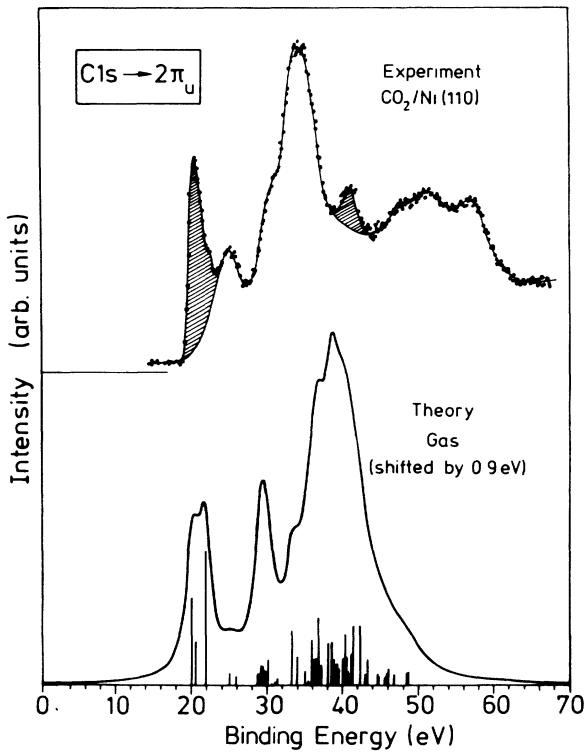

FIG. 4. Direct comparison between measured and calculated autoionization spectra after C $1s \rightarrow 2\pi_u$ excitation. The calculated spectrum has been shifted by 0.9 eV to lower binding energy.

to originate from the $1\pi_g^{-2}2\pi_u$ configuration. The small peak with maximum at 21.5 eV (see Table III) is assigned to these states. In the range 27–28 eV the calculated spectrum exhibits a broad structure which represents the envelope of 15 states situated very close in energy. Figure 5 contains a detailed assignment of the calculated intensities to specific 2h1p configurations. Each symmetry is shown on a separate panel. The states belong to either $^2\Sigma_{g,u}$ or $^2\Delta_{g,u}$ symmetries, and originate from configurations where a $1\pi_g^{-1}2\pi_u$ electron-hole pair or a $1\pi_u^{-1}2\pi_u$ electron-hole pair is coupled to a $4\sigma_g^{-1}$ or a $3\sigma_u^{-1}$ hole. Singlet coupling in the electron-hole pair dominates over triplet coupling. The comparison with the experimental data suggests that the observed shoulder at 26.5 eV should be assigned to this feature. Above 30-eV binding energy we calculate a manifold of autoionization lines, and it appears very difficult to assign a certain group of states to an observed spectral feature. The global maximum of the experimental autoionization spectrum is situated at 30.4 eV, whereas the calculated global maximum is shifted to considerably higher energy, namely approximately 37 eV. Clearly, the calculated maximum strongly depends on the linewidth of the Lorentzian chosen to convolute the calculated line spectra. Since it is not obvious that the linewidth has to be constant, the comparison of the intensity maxima is not particularly meaningful. We shall therefore concentrate on a discussion of the most prominent single contributing states in this energy range. Those states have either $^2\Sigma_{g,u}$ or $^2\Pi_u$ symmetry. States of $^2\Pi_g$ symmetry do not contribute due to symmetry requirements as discussed in connection with the autoionization rate of the single-hole states. The configurations contributing to these states are inner valence single-particle states $2\sigma_u^{-1}$ and $3\sigma_g^{-1}$ and 2h1p states where $\pi^{-1}\pi^*$ electron-hole pairs are coupled to the former single-hole configurations. In addition, there are contributions from $3\sigma_u^{-2}2\pi_u$, $4\sigma_g^{-2}2\pi_u$, and $1\pi_u^{-2}2\pi_u$ configurations. The latter configurations lead to $^2\Pi_u$ states. Experimentally, we find beneath the broad, intense feature a well-resolved peak close to 37 eV. This peak closely aligns with the remnants of the single-hole $2\sigma_u^{-1}$ and $3\sigma_g^{-1}$ states, and it is very tempting to propose this as an assignment. Above 40-eV binding energy three very broad features are found experimentally. A final assignment in this region on the basis of calculations is not possible at the moment. Note, however, that these bands reside considerably above the double-ionization continuum threshold. It is therefore quite likely that these states can be assigned on the basis of the CO_2 Auger spectrum reported by Moddeman *et al.*[36] These authors report intense Auger transitions at double-hole binding energies, i.e., the difference between core-hole binding energy and measured kinetic energy, which are included in Table III for comparison with the binding energies determined via autoionization. Obviously, the observed peaks correlate with the Auger energies. However, the intensities determined in Auger spectroscopy differ from those observed in the present autoionization spectra. This is not surprising, because the decay starts from an excited state of the neutral, and not from the core ionized state as in Auger

spectroscopy. It corresponds to a transition from the left panel to the right panel in Fig. 1, and thus is a three-electron process. Several calculations have been performed to assign the double-ion states. We shall come back to the assignment of these double-ion states after the discussion of the O $1s \rightarrow 2\pi_u$ autoionization decay.

Again, we adopt the same procedure for the discussion of the O $1s \rightarrow 2\pi_u$ autoionization spectrum as was used for the C $1s \rightarrow 2\pi_u$ autoionization spectrum. The spectrum is shown at the top of Fig. 2.

First we investigate the energetic region of the single-hole states. If there is any intensity at all, it is very low, and there are basically no pronounced features visible. At first glance this is a very surprising result, because all

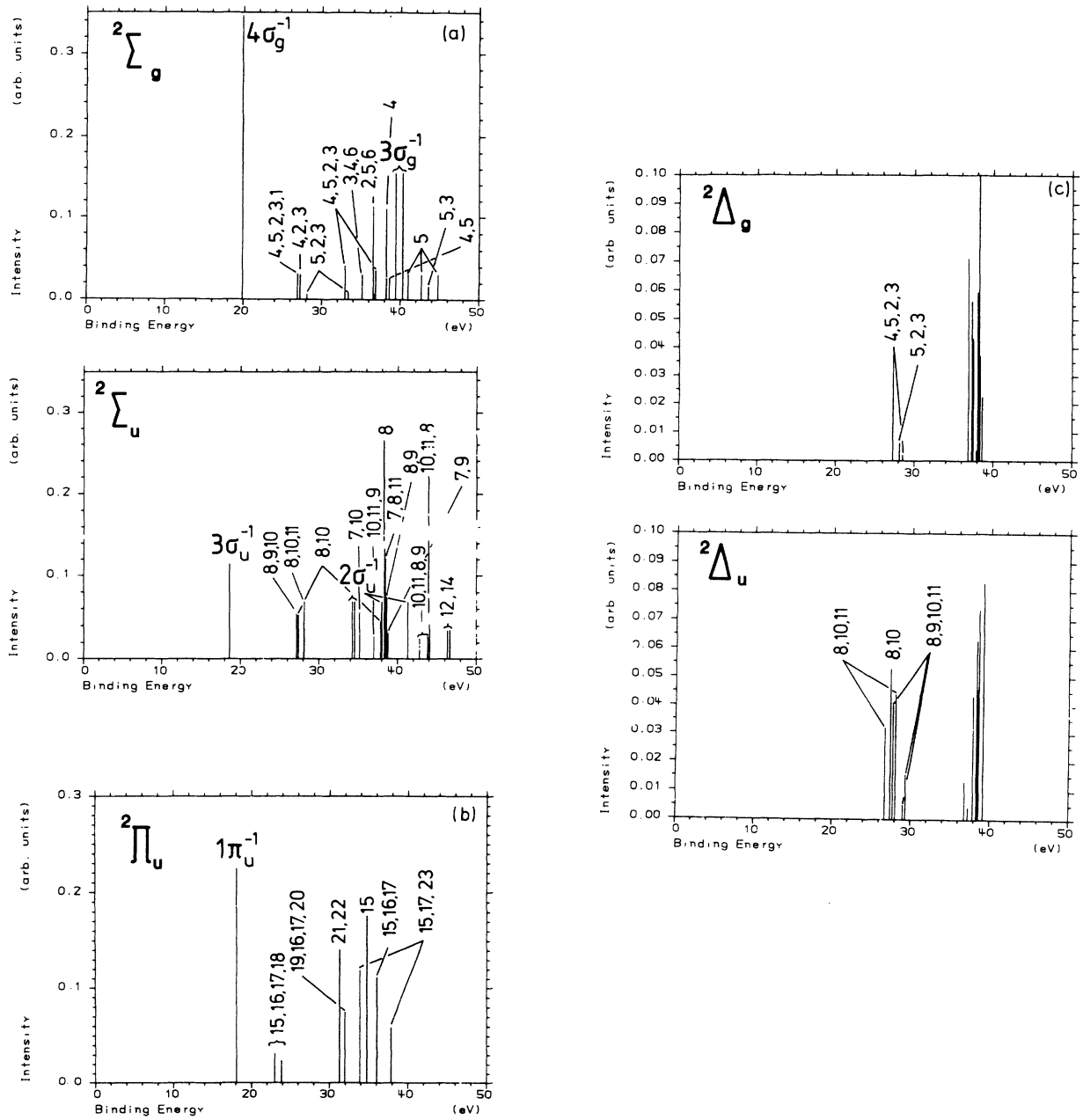

FIG. 5. (a) Calculated autoionization intensities after C $1s \rightarrow 2\pi$ excitation into final ion states of $^2\Sigma_g$ and $^2\Sigma_u$ symmetry. The main configurations contributing to the ion states are given. (b) Calculated autoionization intensities after C $1s \rightarrow 2\pi$ excitation into final ion states of $^2\Pi_u$ symmetry. The main configurations contributing to the ion states are given. The $^2\Pi_g$ states are forbidden by symmetry as discussed in the text. (c) Calculated autoionization intensities after C $1s \rightarrow 2\pi$ excitation into final ion states of $^2\Delta_g$ and $^2\Delta_g$ symmetry. The main configurations contributing to the ion states are given for some states.

valence ion states contain oxygen character, and therefore in contrast to the carbon spectra we had expected to find peaks due to spectator decay into all four valence ion states. There are several reasons for this interesting behavior. One can be found via analysis of the calculated autoionization spectrum shown at the top of Fig. 3. Unlike the case of C $1s \rightarrow 2\pi_u$ autoionization, where the core hole is created at the center of symmetry, and thus does not lead to a left-right distortion of the wave function, the creation of the O $1s \rightarrow 2\pi_u$ hole pair is equivalent to creation of a COF "equivalent-core" molecule, which no longer has a center of symmetry. Clearly, there are two degenerate localized "FCO" and "OCF" states. The one-electron wave functions of these COF molecules are strongly polarized in the sense that the occupied orbitals are more localized on the "core-hole" site, while the unoccupied ones are more localized on the "neutral" oxygen site. Since the decay is determined by the overlap of the valence orbitals with the core-hole site, the autoionization rate for the spectator electron, which resides in an "unoccupied" orbital, decreases considerably. This is verified in the calculated spectra by the relatively weak intensities in the single-particle region, and clearly revealed via the direct comparison of measured and calculated spectra as shown in Fig. 6. Note that the $1\pi_g^{-1}$ state does show a little intensity since it is not forbidden by symmetry. If we compare our calculated spectra with the measured spectrum in Fig. 2 we realize that the observed intensity is even lower than the calculated one. However, a comparison with the corresponding spectrum in the gas phase taken by Thomas[39] shows that the calculated intensities are of the correct order of magnitude. The fact that we are dealing with a molecular solid rather than an isolated molecule may cause this effect. In such a molecular solid, the electronic ion states show energy dispersions as a function of crystal momentum, as has been demonstrated for physisorbed CO_2 by Bartos *et al.*[17] Consequently, the ion states are even more delocalized in the solid as compared to the isolated molecule, and therefore the linewidth increases even further.

Yet another effect has to be taken into account. So far we have only considered the electronic part of the transition rate, neglecting vibrational coupling. However, even for small molecules, it has been shown that the linewidths and shapes in autoionization bands after core-to-bound excitation are drastically dependent on vibrational coupling and lifetime effects in the initial and final states in-

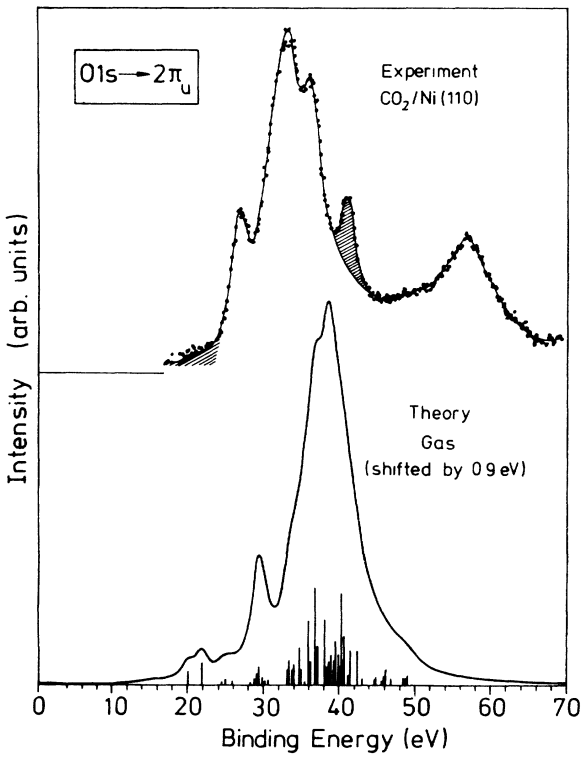

FIG. 6. Direct comparison between measured and calculated autoionization spectra after O $1s \rightarrow 2\pi$ excitation. The calculated spectrum has been shifted by 0.9 eV to lower binding energy.

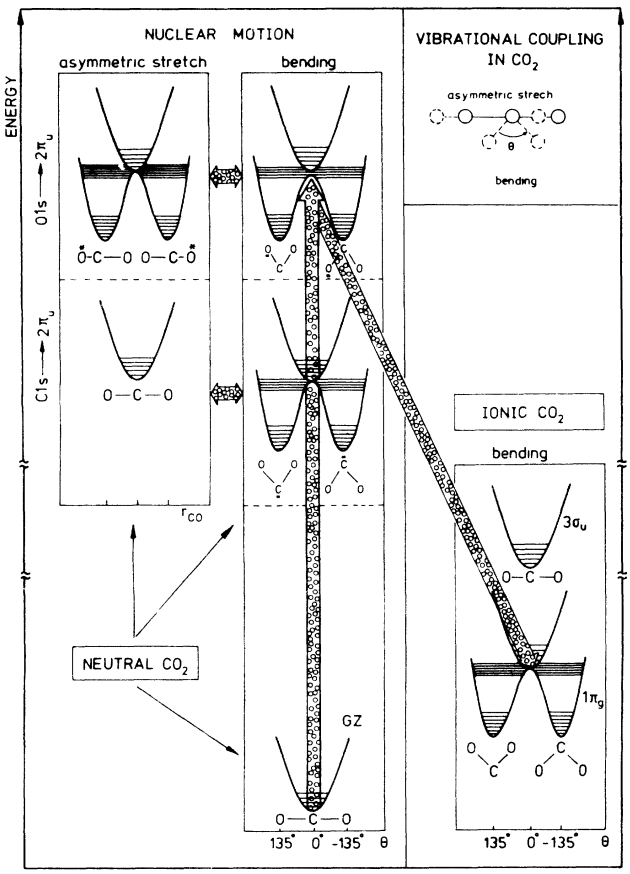

FIG. 7. Schematic representation of the coupling between electronic excitation and vibrational motion in the neutral ground state, the core-to-bound excited state, and the valence ionized states.

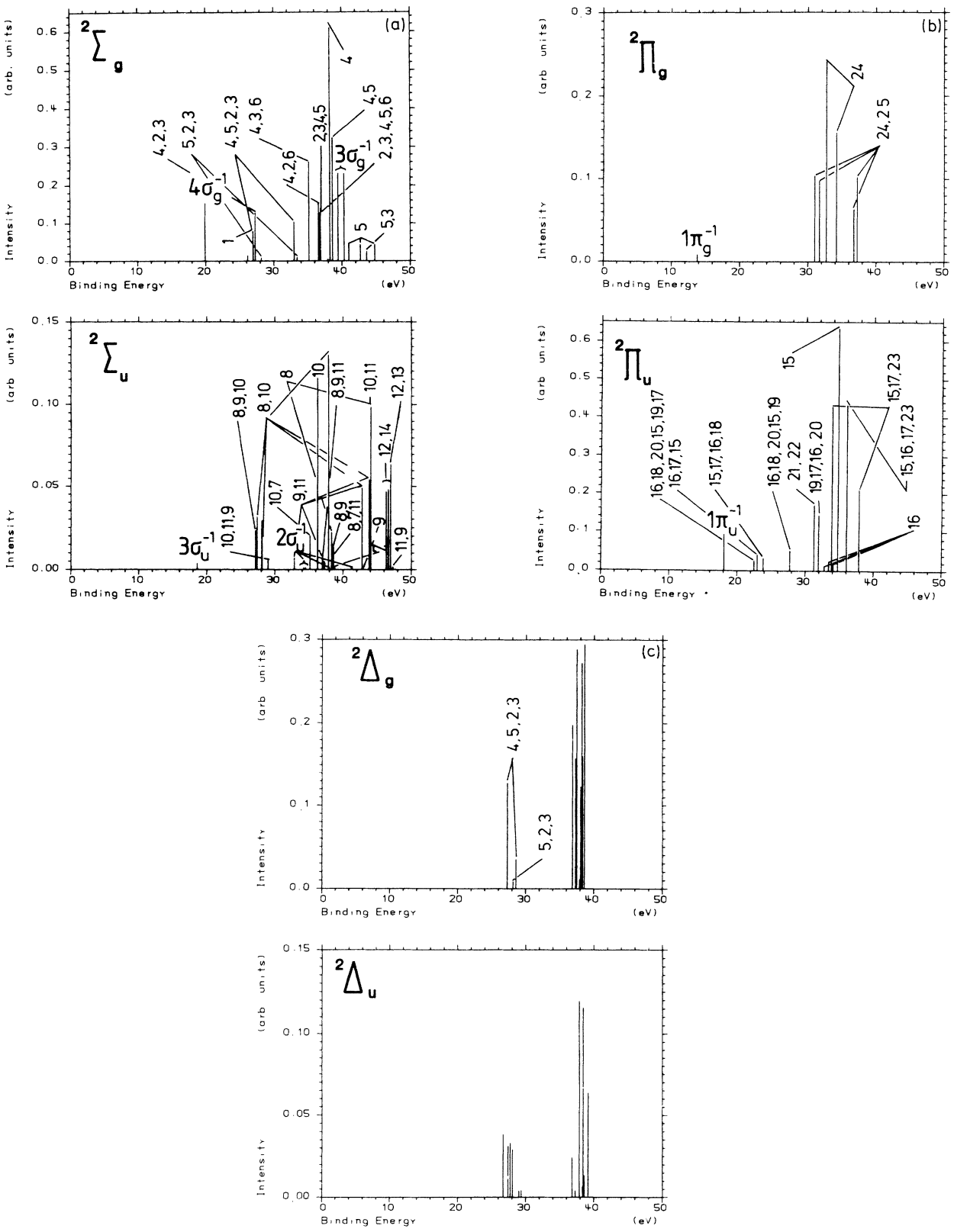

FIG. 8. (a) Calculated autoionization intensities after O $1s \rightarrow 2\pi_u$ excitation into final ion states of $^2\Sigma_g$ and $^2\Sigma_u$ symmetry. The main configurations contributing to the ion states are given. (b) Calculated autoionization intensities after O $1s \rightarrow 2\pi_u$ excitation into final ion states of $^2\Pi_g$ and $^2\Pi_u$ symmetry. The main configurations contributing to the ion states are given. (c) Calculated autoionization intensities after O $1s \rightarrow 2\pi_u$ excitation into final ion states of $^2\Delta_g$ and $^2\Delta_u$ symmetry. The main configurations contributing to the ion states are given for some states.

volved in the radiationless decay.[40] By analyzing their influence, the study of autoionization, in principle, allows us to deduce information about the competition between electronic and vibrational decay in core-to-bound excited states.[9] Figure 7 shows a schematic representation of the potential-energy surfaces of the ground state, the two core-to-bound excited neutral states, and two low-lying ionic states of CO_2. We have chosen the bending coordinate to represent the main distortion of the molecule upon excitation. The bending distortion is due to the well-known Renner-Teller effect[41] accompanying the creation of an electron or a hole in a degenerate π orbital of CO_2. This effect has been discussed in detail for photoionization and electronic excitation of CO_2 by several groups.[38,42,43] The bending angle can be estimated to be in the neighborhood of 135°.[38] Taking vibrational coupling into account, the intensity observed in the autoionization spectrum is then a function of the energy spanned over all possible transitions between vibrational levels of the initial state for the decay and the final ion states. As has been discussed in detail by Cederbaum and Domcke,[42] and by Clark and Müller[43] for the similar case of O 1*s* core ionization in CO_2, the fact that there are two degenerate localized states leads to coupling of the antisymmetric stretching mode. This coupling occurs in addition to the coupling of the bending mode, which is due to the above-discussed Renner-Teller effect. The potential-energy surface in the O $1s \rightarrow 2\pi_u$ excited state therefore shows double-minimum potentials in both normal coordinates. As a consequence, the equilibrium geometry of the O $1s \rightarrow 2\pi_u$ excited state is a bent CO_2 species with two inequivalent C—O bonds. The C—O bond involving the excited oxygen is shorter than the other one, and shorter than the C—O bond length in ground-state CO_2. These vibrational coupling effects spread out the autoionization intensity over a considerable interval. This can also be recognized in the gas-phase autoionization spectra after O $1s \rightarrow 2\pi_u$ excitation reported by Thomas,[39] where the normal-hole states exhibit very broad low intense bands. The intensity is considerably less peaked than in the case of O $1s \rightarrow 2\pi$ decay in CO, where these effects do not occur. Upon condensation of CO_2 into a molecular solid, the band widths of the autoionizations into the normal single-hole states increase even further so that there is hardly any intensity found in the experimental spectrum in Fig. 2 (see also Fig. 6). It is clear that such effects cannot occur in the case of the C $1s \rightarrow 2\pi_u$ excited state, where the electron-hole pair is created on the central carbon atom.

While there are pronounced differences between the decay of the O $1s \rightarrow 2\pi_u$ excitation and C $1s \rightarrow 2\pi_u$ excitations in the regime of normal-hole states, the situation in the regime of the 2h1p ion states is rather similar. The overall shape of the calculated spectrum after Lorentzian convolution is very similar in both cases (Fig. 3). Only a more detailed discussion of the main autoionizing states reveals some differences between O 1*s* and C 1*s* excitation. The broad feature between 25- and 30-eV binding energy is basically due to the same states as in the case of the C $1s \rightarrow 2\pi_u$ excitation. In the energy region above 30-eV binding energies there are two states that exhibit considerably higher intensities than the rest of the states (see Fig. 6). In Fig. 8 the detailed assignment of the calculated intensities is given. The state at approximately 35-eV binding energy is dominated by a $1\pi_u^{-2}2\pi_u$ configuration and gives rise to a $^2\Sigma_u$ state, the second one at around 38 eV has $4\sigma_g^{-1}1\pi_u^{-1}2\pi_u$ character and is a $^2\Sigma_g$ state. Between 31 and 34 eV a set of $^2\Pi_g$ states with considerable intensities is found. The relatively high intensities of these states is characteristic for O $1s \rightarrow 2\pi_u$ autoionization because, as discussed above, $^2\Pi_g$ states are symmetry forbidden in the case of C $1s \rightarrow 2\pi_u$ autoionization. Also, the $^2\Delta_{g,u}$ states are more intense in the former case. The inner valence single-hole states, i.e., the $2\sigma_u^{-1}$ and $3\sigma_g^{-1}$ states, also exhibit considerably higher intensities for the oxygen decay as compared with the carbon decay.

If we now try to assign the experimentally observed features on the basis of our calculations, we find, as in the case of the carbon decay, that the states with higher intensities are calculated at too-high binding energies. However, the calculated intensity pattern strongly suggests that the splitting in the global maximum of the autoionization spectrum is caused by the two most intense states originating from the $1\pi_u^{-2}2\pi_u$ and $4\sigma_g^{-1}1\pi_u^{-1}2\pi_u$ configurations. The $^2\Pi_g$ states, which are characteristic for the oxygen decay, may contribute to the higher intensity of the peak at lower binding energy.

V. SUMMARY AND CONCLUSIONS

We have presented the autoionization spectra after C $1s \rightarrow 2\pi_u$ and O $1s \rightarrow 2\pi_u$ excitation (taken at the storage ring BESSY, Berlin) of CO_2 physisorbed on a Ni(110) surface. The data are compared with the photoelectron spectrum of gaseous and condensed CO_2. To interpret, analyze, and assign the spectra we have carried out *ab initio* Green's-function calculations of the photoelectron as well as the autoionization spectra of CO_2. Briefly, the main results can be summarized as follows.

(1) The fact that photoelectron spectra are governed by dipole selection rules, while autoionization spectra are determined by the Coulomb interaction, documents itself in the spectra. The relative intensities of the ion states in the spectra completely change when going from photoemission to autoionization. This allows a more detailed characterization of ion states.

(2) The comparison of autoionization states after core-to-bound excitations localized at different sites of a molecule allows one to extract information about the distribution of valence electrons in the system. This fact holds a lot of potential, for example in connection with the study of molecular adsorption at surfaces.

(3) It is very important to consider the screening of the core hole created in the excitation process. The intensities of the spectator lines, especially, are very sensitive to asymmetries in the wave functions introduced via screening.

(4) Vibrational coupling can play an important role in the determination of the observed linewidths.

(5) In order to reach satisfactory agreement between experimental and computed spectra, relatively large-scale calculations are necessary, in particular in the calculations of the binding energies of the high-lying ion states in the inner-valence region. It appears that the one-center approximation to the radiationless decay rates gives qualitatively reasonable answers.

We conclude by stating that autoionization may prove a useful supplementary spectroscopy to study adsorbate systems in the future. Via the comparison of decay channels originating from excitations at different positions within a given system, one should be able to get unique spectroscopic information about the distribution of valence electrons in the adsorbate. Autoionization spectroscopy has the advantage over Auger spectroscopy that the final state is the same as in photoelectron spectroscopy, thus allowing direct comparison of the two electron spectroscopic methods. A disadvantage, of course, is the fact that to study autoionization one is bound to use tunable XUV radiation, i.e., to use synchrotron radiation.

ACKNOWLEDGMENTS

The present work was financially supported in part by the "Bundesministerium für Forschung und Technologie" under Project 05-363-FAB-03. Also, the authors are grateful to the Fonds der Chemischen Industrie for support.

*Present address: Lehrstuhl für Physikalische Chemie I, Ruhr-Universität Bochum, 4630 Bochum 1, Federal Republic of Germany.

[1]For discussions of the effects, see L. S. Cederbaum, W. Domcke, J. Schirmer, and W. v. Niessen, Adv. Chem. Phys. **65**, 115 (1986).

[2]H.-J. Freund, H. Kossmann, and V. Schmidt, Chem. Phys. Lett. **123**, 463 (1986).

[3]J. N. Miller, D. T. Ling, I. Lindau, P. M. Stefan, and W. E. Spicer, Phys. Rev. Lett. **38**, 1419 (1977).

[4]H.-J. Freund, F. Grueter, D. Heskett, and E. W. Plummer, Phys. Rev. B **28**, 1727 (1983).

[5]A. Nilsson and N. Mårtensson (unpublished); A. Nilsson, Ph.D. thesis, Uppsala University, Uppsala, 1988.

[6]G. Loubriel, T. Gustafsson, L. I. Johansson, and S. J. Oh, Phys. Rev. Lett. **49**, 571 (1982).

[7]C. T. Chen, Ph.D. thesis, University of Pennsylvania, 1985.

[8]E. W. Plummer, C. T. Chen, W. K. Ford, W. Eberhardt, R. P. Messmer, and H.-J. Freund, Surf. Sci. **158**, 58 (1985).

[9]W. Eberhardt, Phys. Sci. **T 17**, 28 (1987).

[10]D. Menzel, P. Feulner, R. Treichler, E. Umbach, and W. Wurth, Phys. Sci. **T 17**, 166 (1987).

[11]W. Wurth, C. Schneider, R. Treichler, E. Umbach, and D. Menzel, Phys. Rev. B **35**, 7741 (1987).

[12]W. Wurth, Ph.D. thesis, Universität München, 1987.

[13]W. Wurth, C. Schneider, R. Treichler, D. Menzel, and E. Umbach, Phys. Rev. B **37**, 8725 (1988).

[14]G. Illing, T. Porwol, H.-J. Freund, H. Kuhlenbeck, M. Neumann, and S. Bernstorff, in *Proceedings of the 3rd Surface Science Symposium, Kaprun, Austria* (Varga, Vienna, 1988), p. 81.

[15]H.-J. Freund and M. Neumann, Appl. Phys. A **47**, 3 (1988).

[16](a) L. Ungier and T. D. Thomas, Chem. Phys. Lett. **96**, 247 (1983); Phys. Rev. Lett. **53**, 435 (1984); J. Chem. Phys. **82**, 3146 (1985); (b) M. Jousif, D. E. Ramaker, and H. Sambe, Chem. Phys. Lett. **101**, 472 (1983); (c) U. Becker, R. Hölzel, H.-G. Kerkhoff, B. Lander, B. Szosak, and B. Wehlitz, Phys. Rev. Lett. **56**, 1455 (1986).

[17](a) B. Bartos, H.-J. Freund, H. Kuhlenbeck, M. Neumann, H. Lindner, and K. Müller, Surf. Sci. **179**, 59 (1987); (b) J. Wambach, G. Odörfer, H.-J. Freund, H. Kuhlenbeck, and M. Neumann, *ibid.* **209**, 159 (1989).

[18]G. Illing, D. Heskett, E. W. Plummer, H.-J. Freund, J. Somers, Th. Lindner, A. M. Bradshaw, U. Buskotte, M. Neumann, U. Starke, K. Heinz, P. de Andres, D. Saldin, and J. B. Pendry, Surf. Sci. **206**, 1 (1988).

[19]S. Wohlrab, D. Ehrlich, J. Wambach, H. Kuhlenbeck, and H.-J. Freund, Surf. Sci. (to be published).

[20]*Desorption Induced by Electronic Transitions, DIET II,* Vol. 4 of *Springer Series in Surface Science,* edited by W. Brenig and D. Menzel (Springer, Heidelberg, 1985).

[21]L. S. Cederbaum and W. Domcke, Adv. Chem. Phys. **36**, 205 (1977).

[22]J. Schirmer, L. S. Cederbaum, and O. Walter, Phys. Rev. A **28**, 1237 (1983).

[23]J. Schirmer and L. S. Cederbaum, J. Phys. B **11**, 1889 (1978).

[24]E. R. Davidson, J. Comp. Phys. **17**, 87 (1975); B. Lin, NRCC Report No. LBL 8158, 1978 (unpublished).

[25]F. Tarantelli (private communication). In the calculations we used a program of F. Tarantelli.

[26]W. v. Niessen, J. Schirmer, and L. S. Cederbaum, Comput. Phys. Rep. **1**, 39 (1984).

[27]C. Salez and A. Veillard, Theor. Chim. Acta **11**, 441 (1968).

[28]G. H. F. Diercksen and W. P. Kraemer, MUNICH, Molecular Program System, Special Technical Report, Max-Planck-Institut für Astrophysik (unpublished); G. H. F. Diercksen, Theor. Chim. Acta **33**, 1 (1974).

[29]W. Domcke, L. S. Cederbaum, J. Schirmer, W. V. Niessen, C. E. Brion, and K. H. Tan, Chem. Phys. **40**, 171 (1979).

[30]G. Wentzel, Z. Phys. **43**, 524 (1927).

[31](a) H.-J. Freund and C.-M. Liegener, Chem. Phys. Lett. **134**, 70 (1987); (b) T. Porwol, Diplomarbeit, Ruhr-Universität Bochum, 1989.

[32]H. Siegbahn, L. Asplund, and P. Kelfve, Chem. Phys. Lett. **35**, 330 (1975).

[33]E. J. McGuire, Phys. Rev. **185**, 1 (1969).

[34]W. L. Jolly and D. N. Hendrickson, J. Am. Chem. Soc. **92**, 1863 (1970).

[35]D. W. Davis and D. A. Shirley, Chem. Phys. Lett. **15**, 185 (1972).

[36]W. Moddeman, T. A. Carlson, M. O. Krause, B. P. Pullen, W. E. Bull, and G. K. Schweitzer, J. Chem. Phys. **55**, 2317 (1971).

[37]J.-H. Fock, H.-J. Lau, and E. E. Koch, Chem. Phys. **83**, 377 (1984).

[38]G. R. Wight and C. E. Brion, J. Electron. Spectrosc. Relat.

Phenom. **3**, 191 (1974).
[39]T. D. Thomas (private communication).
[40]N. Correira, A. Flores-Riveros, H. Ågren, K. Helenelund, C. Asplund, and U. Gelius, J. Chem. Phys. **83**, 2035 (1985).
[41](a) G. Herzberg and E. Teller, Z. Phys. Chem. B **21**, 410 (1933); (b) R. Renner, Z. Phys. **92**, 172 (1934).
[42]W. Domcke and L. S. Cederbaum, Chem. Phys. **25**, 189 (1977).
[43]D. T. Clark and J. Müller, Chem. Phys. **23**, 429 (1977).